

RESEARCH ARTICLE

Comet 81P/Wild 2 Under a Microscope

Don Brownlee,¹ Peter Tsou,² Jérôme Aléon,^{3,4} Conel M. O'D. Alexander,⁵ Tohru Araki,⁶ Sasa Bajt,⁷ Giuseppe A. Baratta,⁸ Ron Bastien,⁹ Phil Bland,^{10,11} Pierre Bleuet,¹² Janet Borg,¹³ John P. Bradley,¹⁴ Adrian Brearley,¹⁵ F. Brenker,¹⁶ Sean Brennan,¹⁷ John C. Bridges,¹⁸ Nigel D. Browning,^{19,20} John R. Brucato,²¹ E. Bullock,²² Mark J. Burchell,²³ Henner Busemann,⁵ Anna Butterworth,²⁴ Marc Chaussidon,²⁵ Allan Cheuvront,²⁶ Miaofang Chi,¹⁴ Mark J. Cintala,²⁷ B. C. Clark,²⁶ Simon J. Clemett,²⁸ George Cody,²⁹ Luigi Colangeli,²¹ George Cooper,³⁰ Patrick Cordier,³¹ C. Daghlán,³² Zurong Dai,¹⁴ Louis D'Hendecourt,¹³ Zahia Djouadi,¹³ Gerardo Dominguez,³³ Tom Duxbury,² Jason P. Dworkin,³⁴ Denton S. Ebel,³⁵ Thanasis E. Economou,³⁶ Sirine Fakra,³⁷ Sam A. J. Fairey,³⁸ Stewart Fallon,¹⁴ Gianluca Ferrini,³⁹ T. Ferroir,⁴⁰ Holger Fleckenstein,⁴¹ Christine Floss,⁴² George Flynn,⁴³ Ian A. Franchi,⁴⁴ Marc Fries,²⁹ Z. Gainsforth,²⁴ J.-P. Gallien,⁴⁵ Matt Genge,⁴⁶ Mary K. Gilles,⁴⁷ Philippe Gillet,⁴⁰ Jamie Gilmour,⁴⁸ Daniel P. Glavin,³⁴ Matthieu Gounelle,^{49,10} Monica M. Grady,¹⁸ Giles A. Graham,¹⁴ P. G. Grant,¹⁴ Simon F. Green,¹⁸ Faustine Grossey,¹³ Lawrence Grossman,^{36,50} Jeffrey N. Grossman,⁵¹ Yunbin Guan,⁵² Kenji Hagiya,¹⁰ Ralph Harvey,⁵³ Philipp Heck,⁵⁴ Gregory F. Herzog,⁵⁵ Peter Hoppe,⁵⁴ Friedrich Hörz,⁵⁶ Joachim Huth,⁵⁴ Ian D. Hutcheon,⁴ Konstantin Ignatyev,⁵⁷ Hope Ishii,¹⁴ Motoso Ito,⁵⁸ Damien Jacob,⁵⁹ Chris Jacobsen,⁶⁰ Stein Jacobsen,⁶¹ Steven Jones,² David Joswiak,¹ Amy Jurewicz,⁶² Anton T. Kearsley,¹⁰ Lindsay P. Keller,⁵⁶ H. Khodja,⁴⁷ A.L. David Kilcoyne,^{37,47} Jochen Kissel,⁶³ Alexander Krot,⁶⁴ Falko Langenhorst,⁶⁵ Antonio Lanzirotti,⁶⁶ Loan Le,⁶⁷ Laurie A. Leshin,⁶⁸ J. Leitner,⁶⁹ L. Lemelle,⁴⁰ Hugues Leroux,⁷⁰ Ming-Chang Liu,⁷¹ K. Luening,¹⁷ Ian Lyon,⁴⁸ Glen MacPherson,²² Matthew A. Marcus,³⁷ Kuljeet Marhas,⁷² Bernard Marty,⁷³ Graciela Matrajt,¹ Kevin McKeegan,⁷¹ Anders Meibom,⁴⁸ Vito Mennella,⁷⁴ Keiko Messenger,⁹ Scott Messenger,⁵⁸ Takashi Mikouchi,⁷⁵ Smail Mostefaoui,⁷⁶ Tomoki Nakamura,⁷⁷ T. Nakano,⁷⁸ M. Newville,⁶⁶ Larry R. Nittler,⁵ Ichiro Ohnishi,⁷⁹ Kazumasa Ohsumi,⁸⁰ Kyoko Okudaira,⁸¹ Dimitri A. Papanastassiou,⁸² Russ Palma,^{83,84} Maria E. Palumbo,⁸ Robert O. Pepin,⁸⁴ David Perkins,²⁶ Murielle Perronnet,⁵⁶ P. Pianetta,⁵⁷ William Rao,⁸⁵ Frans J. M. Rietmeijer,¹⁵ François Robert,⁴⁹ D. Rost,²² Alessandra Rotundi,⁸⁶ Robert Ryan,² Scott A. Sandford,⁸⁷ Craig S. Schwardt,¹³ Thomas H. See,⁸⁸ Dennis Schlutter,⁸³ J. Sheffield-Parker,⁸⁹ Alexandre Simionovici,⁵⁴ Steven Simon,⁵⁰ I. Sitnitsky,⁹⁰ Christopher J. Snead,²⁴ Maegan K. Spencer,⁹⁶ Frank J. Stadermann,⁴² Andrew Steele,²⁹ Thomas Stephan,⁶⁹ Rhonda Stroud,⁸⁹ Jean Susini,¹⁴ S. R. Sutton,^{50,66} Y. Suzuki,⁹¹ Mitra Taheri,⁸⁷ Susan Taylor,⁹² Nick Teslich,¹⁴ Kazu Tomeoka,⁷⁷ Naotaka Tomioka,⁷⁷ Alice Toppini,^{3,14} Josep M. Trigo-Rodríguez,^{93,94} David Troadec,⁶⁸ Akira Tsuchiyama,⁹⁵ Anthony J. Tuzzolino,³⁴ Tolek Tyliczszak,^{35,45} K. Uesugi,⁹⁶ Michael Velbel,⁹⁷ Joe Vellenga,²⁶ E. Vicenzi,²² L. Vincze,⁹⁸ Jack Warren,⁹ Iris Weber,⁶⁹ Mike Weisberg,⁹⁹ Andrew J. Westphal,²⁴ Sue Wirick,⁴¹ Diane Wooden,⁸⁷ Brigitte Wopenka,^{72,100} Penelope Wozniakiewicz,¹⁰ Ian Wright,¹⁸ Hikaru Yabuta,²⁹ Hajime Yano,⁸¹ Edward D. Young,⁷¹ Richard N. Zare,⁹⁶ Thomas Zega,⁸¹ Karen Ziegler,⁷¹ Laurent Zimmerman,²⁵ Ernst Zinner,⁴² Michael Zolensky⁵⁶

The Stardust spacecraft collected thousands of particles from comet 81P/Wild 2 and returned them to Earth for laboratory study. The preliminary examination of these samples shows that the nonvolatile portion of the comet is an unequilibrated assortment of materials that have both presolar and solar system origin. The comet contains an abundance of silicate grains that are much larger than predictions of interstellar grain models, and many of these are high-temperature minerals that appear to have formed in the inner regions of the solar nebula. Their presence in a comet proves that the formation of the solar system included mixing on the grandest scales.

Stardust was the first mission to return solid samples from a specific astronomical body other than the Moon. The mission, part of the NASA Discovery program, retrieved samples from a comet that is believed to have formed at the outer fringe of the solar nebula, just beyond the most distant planet. The samples, isolated from the planetary region of the solar system for billions of years, provide new insight into the formation of the

solar system. The samples provide unprecedented opportunities both to corroborate astronomical (remote sensing) and sample analysis information (ground truth) on a known primitive solar system body and to compare preserved building blocks from the edge of the planetary system with sample-derived and astronomical data for asteroids, small bodies that formed more than an order of magnitude closer to the Sun. The asteroids, parents of most

meteorites, formed by accretion of solids in warmer, denser, more collisionally evolved inner regions of the solar nebula where violent nebular events were capable of flash-melting millimeter-sized rocks, whereas comets formed in the coldest, least dense region. The samples collected by Stardust are the first primitive materials from a known body, and as such they provide contextual insight for all primitive meteoritic samples. About 200 investigators around the world participated in the preliminary analysis of the returned samples, and the papers in this issue summarize their findings.

Observations. During its 2 January 2004 flyby, 234 km from the surface of comet Wild 2, Stardust collected more than 10,000 particles in the 1-to 300- μ m size range that were returned to Earth on 15 January 2006 (*1*). Flyby images showed at least 20 collimated jets of solid particles streaming into space from widely distributed small sources (*2*). The collected particles are expected to be a representative sampling of the nonvolatile component of the interior of the comet. Wild 2 is a Jupiter family comet (JFC) currently on an orbit that approaches the orbits of both Jupiter and Mars. Like other JFCs, this ~4.5-km-diameter body is believed to have formed in the Kuiper belt, exterior to the orbit of Neptune, and only recently entered the inner regions of the solar system where solar heat causes “cometary activity,” processes mainly driven by the sublimation of water ice that lead to the loss of gas, rocks and dust at rates of tons per second. As a JFC, the most likely history of Wild 2 is that it formed beyond Neptune, where it spent nearly all of its life orbiting in the Kuiper belt. A close encounter with Jupiter on 10 September 1974 placed it in its current orbit, but its journey from the Kuiper belt to the inner solar system probably took millions of years and multiple encounters with outer planets. As a JFC, its orbit will change, and it has an expected dynamical lifetime of ~ 10^4 years before it either hits a larger object or is ejected from the solar system (*3*). The active lifetime will be shorter because of mass loss or disintegration.

The particles ejected by the comet and collected by Stardust should be the same materials that accreted along with ices to form the comet ~4.57 billion years ago when the Sun and planets formed. The original accreted materials included both fine nebular particles and compounds from the disruption of large bodies (*4*). Cometary activity has caused Wild 2 to lose its original surface, and for this and other reasons it is believed that all of the particles ejected by the comet date back to the formational period of the solar system history and not to recent solar system processes. Exposed to space for hours before collection, solar heating at 1.86 AU probably volatilized ice components during transit from Wild 2 to the spacecraft, although it is possible that some ice could have been retained

in the largest particles. The fact that particles ranging down to submicron size were ejected by such a gentle process as ice sublimation indicates that the collected material from Wild 2 had not been lithified and altered in Wild 2 by internal processes such as heating, compaction, or aqueous alteration. These processes did act on original asteroidal materials, altering them into relatively dense and strong rocks that could survive entry into the atmosphere, impact the ground and be found as meteorites.

Collection of particles. Most of the samples were collected in silica aerogel, a porous glass composed of nanometer-sized silica particles with bulk density that was made to vary from $<0.01 \text{ g/cm}^3$ at the impact surface to 0.05 g/cm^3

at 3-cm depth. In addition to aerogel, about 15% of the total collection surface was aluminum, the frame used to hold aerogel. Impact on this metal produced bowl-shaped craters lined with melted, and in some cases unmelted, projectile residue. The craters provide important information that is complementary to the primary aerogel collection medium. The impacts into aerogel produced deep, tapered cavities (tracks) with shapes varying with the nature of the impacting particle (Fig. 1). All but a few of the impact tracks contain deeply penetrating particles. Nonfragmenting particles produced carrot-shaped tracks with length/diameter ratios of >25 , whereas fragmenting particles produced tracks with bulbous upper regions and sometimes multiple roots. In

many cases, as described by Hörz *et al.* (5), it appears that the particles consisted of aggregates that separated into fragments on impact. The smaller fragments stopped in the upper (bulbous) region of the tracks, whereas the larger fragments traveled deeper into the aerogel. The upper parts of the hollow tracks are lined with relatively large amounts of melted aerogel with dissolved projectile, the mid-regions contain less melt and more preserved projectile material along with compressed aerogel, and the lower regions contain largely unmelted comet fragments at the track ends. In the majority of cases, the deepest penetrating particles are solid mineral grains or rocks composed of multiple components. To date, no terminal particles have been found that

¹Department of Astronomy, University of Washington, Seattle, WA 98195, USA. ²Jet Propulsion Laboratory, California Institute of Technology, Pasadena CA 91109–8099, USA. ³Centre de Spectrométrie Nucléaire et de Spectrométrie de Masse, Bat 104, 91405 Orsay Campus, France. ⁴Glenn T. Seaborg Institute, Lawrence Livermore National Laboratory, Livermore, CA 94550, USA. ⁵Department of Terrestrial Magnetism, Carnegie Institution, Washington, DC 20015–1305, USA. ⁶Department of Physics, North Carolina State University, Raleigh, NC 27695, USA. ⁷Lawrence Livermore National Laboratory, 7000 East Avenue, L-210, Livermore, CA 94550, USA. ⁸Istituto Nazionale di Astrofisica, Osservatorio Astrofisico di Catania, Via Santa Sofia 78, 95123 Catania, Italy. ⁹Engineering Science Contract Group, NASA Johnson Space Center, Houston, TX 77058, USA. ¹⁰Department of Mineralogy, Natural History Museum, London, SW7 5BD, UK. ¹¹Impact and Astromaterials Research Centre, Department of Earth Sciences and Engineering, Imperial College of Science, Technology, and Medicine, Prince Consort Road, London, SW7 2AZ, UK. ¹²European Synchrotron Research Facility, Grenoble, France. ¹³Institut d'Astrophysique Spatiale, Campus, 91405 Orsay Cedex, France. ¹⁴Institute for Geophysics and Planetary Physics, Lawrence Livermore National Laboratory, Livermore, CA 94550, USA. ¹⁵Department of Earth and Planetary Sciences, University of New Mexico, MSC 03-2040, Albuquerque, NM 87131–0001, USA. ¹⁶Johann Wolfgang Goethe Universität, Frankfurt, Germany. ¹⁷Stanford Linear Accelerator Center, Menlo Park, CA 94025, USA. ¹⁸Planetary and Space Sciences Research Institute, The Open University, Walton Hall, Milton Keynes MK7 6AA, UK. ¹⁹Department of Chemical Engineering and Materials Science, University of California–Davis, Davis, CA 95616, USA. ²⁰Materials Science and Technology Division, Chemistry and Materials Science Directorate, Lawrence Livermore National Laboratory, Livermore, CA 94550, USA. ²¹INAF, Osservatorio Astronomico di Capodimonte, Via Moiriello 16, 80131 Napoli, Italy. ²²Smithsonian Institution, Washington DC, USA. ²³School of Physical Sciences, University of Kent, Canterbury, Kent CT2 7NH, UK. ²⁴Space Sciences Laboratory, University of California, Berkeley, CA 94720–7450, USA. ²⁵Centre de Recherches Petrographiques et Geochimiques, 15 rue Notre Dame des Pauvres, BP 20, 54501 Vandoeuvre lès Nancy, France. ²⁶Lockheed Martin Space Systems, Littleton, CO 80125, USA. ²⁷Astromaterials Research and Exploration Science, NASA Johnson Space Center, Houston, TX 77058, USA. ²⁸ERC, Inc., NASA Johnson Space Center, Houston, TX 77058, USA. ²⁹Geophysical Laboratory, Carnegie Institution of Washington, Washington, DC 20015, USA. ³⁰Exobiology Branch, NASA Ames Research Center, Moffett Field, CA 94035, USA. ³¹Laboratoire de Structure et Propriétés de l'Etat Solide, Bat C6, Université des Sciences et Technologies de Lille, 59655 Villeneuve d'Ascq, France. ³²Dartmouth College, Hanover, NH 03755, USA. ³³Department of Chemistry and Biochemistry, University of California San Diego, 9500 Gilman Drive, La Jolla, CA 92093–0356, USA. ³⁴Goddard Center for Astrobiology, NASA Goddard Space Flight Center, Greenbelt, MD 20771, USA. ³⁵Department of Earth and

Planetary Sciences, American Museum of Natural History, New York, NY 10024, USA. ³⁶Laboratory for Astrophysics and Space Research, Enrico Fermi Institute, University of Chicago, 933 East 56th Street, Chicago, IL 60637, USA. ³⁷Advanced Light Source, Lawrence Berkeley National Laboratory, Berkeley, CA 94720–8225, USA. ³⁸Centre for Astrophysics and Planetary Sciences, University of Kent, Canterbury, Kent CT2 7NH, UK. ³⁹Novatech s.r.l., Napoli, Italy. ⁴⁰Laboratoire de Sciences de la Terre, Ecole Normale Supérieure de Lyon, 46, allée d'Italie, 69007, Lyon, France. ⁴¹Physics and Astronomy Department, SUNY at Stony Brook, Stony Brook, NY 11794–3800, USA. ⁴²Laboratory for Space Sciences, CB1105, Washington University, St. Louis, MO 63160–4899, USA. ⁴³Department of Physics, SUNY, Plattsburgh, NY 12901, USA. ⁴⁴Open University, Milton Keynes MK7 6AA, UK. ⁴⁵Laboratoire Pierre Süe, CEA-Saclay 91191 Gif sur Yvette, France. ⁴⁶Impact and Astromaterials Research Centre, Department of Earth Sciences and Engineering, Imperial College of Science Technology and Medicine, London, SW7 2AZ, UK. ⁴⁷Chemical Science Division, Lawrence Berkeley National Laboratory, Berkeley, CA 94720–8225, USA. ⁴⁸School of Earth, Atmospheric and Environmental Sciences, University of Manchester, Manchester, M13 9PL, UK. ⁴⁹Museum National d'Histoire Naturelle, Laboratoire d'Etude de la Matière Extraterrestre, USM 0205 (LEME), Case Postale 52, 57, rue Cuvier, 75005 Paris, France. ⁵⁰Department of the Geophysical Sciences, University of Chicago, 5734 South Ellis Avenue, Chicago, IL 60637, USA. ⁵¹United States Geological Survey, 954 National Center, Reston, VA 20192, USA. ⁵²Division of Geological and Planetary Sciences, California Institute of Technology, Pasadena, CA 91125, USA. ⁵³Geology Department, Case Western Reserve University, Cleveland, OH 44106, USA. ⁵⁴Max Planck Institute for Chemistry, Particle Chemistry Department, P.O. Box 3060, 55020 Mainz, Germany. ⁵⁵Rutgers University, Piscataway NJ, USA. ⁵⁶Astromaterials Research and Exploration Science, NASA Johnson Space Center, Houston, Texas 77058, USA. ⁵⁷Stanford Synchrotron Radiation Laboratory, Stanford Linear Accelerator Center, Menlo Park, CA 94025, USA. ⁵⁸Robert M. Walker Laboratory for Space Science, Astromaterials Research and Exploration Science Directorate, NASA Johnson Space Center, Houston, TX 77058, USA. ⁵⁹Laboratoire de Structure et Propriétés de l'Etat Solide, Bat C6, Université des Sciences et Technologies de Lille, 59655 Villeneuve d'Ascq, France. ⁶⁰Physics and Astronomy Department, SUNY at Stony Brook, Stony Brook, NY 11794–3800, USA. ⁶¹Department of Earth and Planetary Sciences, Harvard University, 20 Oxford Street, Cambridge, MA 02138, USA. ⁶²Center for Meteorite Studies, Arizona State University, m/c 1404, Tempe AZ 85287, USA. ⁶³Max Planck Institut for Solar System Research, Max-Planck-Strasse 2, 37191 Katlenburg-Lindau, Germany. ⁶⁴Hawaii Institute of Geophysics and Planetology, University of Hawaii, Honolulu, HI 96822, USA. ⁶⁵Institute of Geosciences, Friedrich-Schiller-University Jena, Burgweg 11, D-07749 Jena, Germany. ⁶⁶Center for Advanced Radiation Studies, University of Chicago, Chicago, IL 60637, USA. ⁶⁷Jacobs Sverdrup, ESCG, Houston, TX 77058, USA. ⁶⁸Sciences and Exploration Directorate, NASA

Goddard Space Flight Center, Greenbelt, MD 20771, USA. ⁶⁹Institut für Planetologie, Westfälische Wilhelms-Universität, Münster, Germany. ⁷⁰Université Lille, Lille, France. ⁷¹Department of Earth and Space Sciences, University of California Los Angeles, Los Angeles, CA 90095–1567, USA. ⁷²McDonnell Center for the Space Sciences, Department of Physics, Washington University, St. Louis, MO 63130, USA. ⁷³Centre de Recherches Petrographiques et Geochimiques, 15 rue Notre Dame des Pauvres, BP 20, 54501 Vandoeuvre lès Nancy, France. ⁷⁴INAF, Osservatorio Astronomico di Capodimonte, Via Moiriello 16, 80131 Napoli, Italy. ⁷⁵Department of Earth and Planetary Science, University of Tokyo, Hongo, Bunkyo-ku, Tokyo 113-0033, Japan. ⁷⁶Museum National d'Histoire Naturelle, Laboratoire d'Etude de la Matière Extraterrestre, 57 rue Cuvier, 75005, Paris, France. ⁷⁷Kyushu University, Fukuoka, Japan. ⁷⁸Advanced Industrial Science and Technology, Geological Survey of Japan, Ibaragi, Japan. ⁷⁹Department of Earth and Planetary Sciences, Faculty of Science, Kobe University, Nada, Kobe 657-8501, Japan. ⁸⁰Institute of Materials Structure Science, Tsukuba-shi, Ibaraki-ken, 305, Japan. ⁸¹Japan Aerospace Exploration Agency, Institute of Space and Astronautical Science, 3-1-1 Yoshinodai, Sagami-hara, Kanagawa, 229-8510, Japan. ⁸²Science Division, Jet Propulsion Laboratory, 4800 Oak Grove Drive, Pasadena, CA 91109, USA. ⁸³Department of Physics and Astronomy, Minnesota State University, 141 Trafton Science Center N, Mankato, MN 56001, USA. ⁸⁴School of Physics and Astronomy, University of Minnesota, Minneapolis, MN 55455, USA. ⁸⁵Savannah River Ecology Lab, Aiken, SC 29801, USA. ⁸⁶Dip. Scienze Applicate, Università degli Studi di Parthenope, Napoli, Italy. ⁸⁷Astrophysics Branch, NASA Ames Research Center, Moffett Field, CA 94035, USA. ⁸⁸Engineering Science Contract/Barrios Technology, Astromaterials Research and Exploration Science/Johnson Space Center, Houston, Texas 77258–8447, USA. ⁸⁹U.S. Naval Research Laboratory, Washington, DC 20375, USA. ⁹⁰State University of New York, Plattsburgh, NY 12901, USA. ⁹¹Japan Synchrotron Radiation Institute, Hyogo, Japan. ⁹²Engineer Research and Development Center, Cold Regions Research and Engineering Laboratory, Hanover, NH 03755, USA. ⁹³Institute of Space Sciences Institut d'Estudis Espacials de Catalunya, CSIC, Universitat Autònoma de Barcelona, Campus UAB, 08193 Bellaterra (Barcelona), Spain. ⁹⁴Institut d'Estudis Espacials de Catalunya (IEEC), Ed. Nexus, Gran Capità, 2-4, 08034 Barcelona, Spain. ⁹⁵Department of Earth and Space Science, Osaka University, 1-1 Machikaneyama-cho, Toyonaka, 560-0043, Japan. ⁹⁶Department of Chemistry, Stanford University, Stanford, California 94305–5080, USA. ⁹⁷Department of Geological Sciences, Michigan State University, East Lansing, MI 48824–1115, USA. ⁹⁸Ghent Univ, Ghent, Belgium. ⁹⁹Physical Sciences, Kingsborough Community College (CUNY), Brooklyn, NY 11235, USA. ¹⁰⁰Department of Earth and Planetary Sciences, Washington University, St. Louis, MO 63130–4899, USA.

*To whom correspondence should be addressed. E-mail: brownlee@astro.washington.edu

Fig. 1. Optical images of deceleration tracks of eight comet particles in aerogel that entered at the top and terminated at the base. Left to right, the track names and their lengths are T59 (0.35 mm), T58 Noni (0.29 mm), T61 (1.6 mm), T72 Gea (0.12 mm), T71 Surya (0.22 mm), T38 Tara (3.2 mm), T27 Sitara (>2 mm), and T25 Inti (2 mm). The thinner tracks suffered very little fragmentation that leads to substantial production of side tracks. The break in the T38 track is due to sample preparation, and the upper bulb of T25 widened a bit when it was intentionally flattened. All of the other tracks have their original shapes. The squares below T25 (Inti) are magnified images of five of the major 5- to 12- μ m particles. The tip of the track containing the 20- μ m terminal particle was removed before the track image was taken. The terminal particle as well as many of the other fragments are isotopically and mineralogically linked CAIs, exotic refractory components in primitive meteorites that may have formed very close to the young Sun.

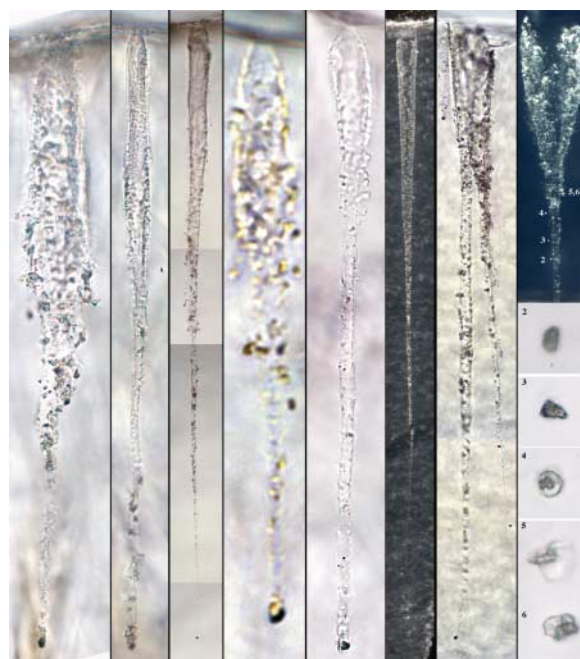
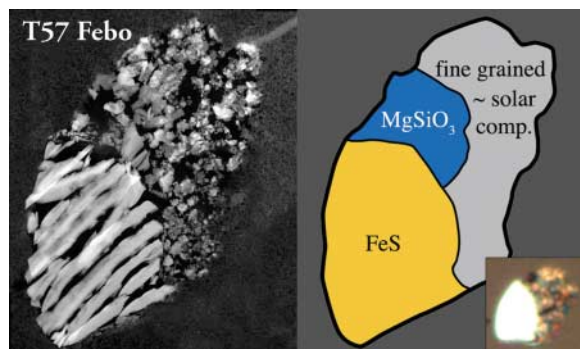


Fig. 2. The 8- μ m terminal particle of T57 (Febo), a bifurcated track >1.4 mm long. The left image is a high-angle annular darkfield (HAADF) image of a 70-nm-thick microtome section of the particle. The images combined with x-ray spectral analysis show that the particle has three major components. The sulfide pyrrhotite on the left, a 3- μ m enstatite grain in the upper middle, and fine-grained porous aggregate material with approximately chondritic elemental composition (Mg, Al, Si, S, Ca, Cr, Mn, Fe, Ni ~ solar ratios) dominates the right half of the image. The particle's smooth exterior contour is probably due to abrasion during passage through aerogel, although the particle contains only trace amounts, at most, of adhering aerogel. The survival of fine-grained chondritic composition material as a major part of a terminal particle is unusual, and its survival may have been aided by shielding; it may have been in the lee of the large sulfide. The small inset image shows a reflected-light view of the "potted butt," the sample that remains after removing microtome sections.



are entirely composed of submicron chondritic composition (Mg, Al, Si, S, Ca, Fe, Ni ratios = solar) materials similar to the material that dominates interplanetary dust and the matrix of primitive carbon-rich meteorites, although such material has been seen attached to terminal particles (Fig. 2).

All the particles were modified to some degree by capture, and recognizing and developing a better understanding of the effects is important for understanding the properties of the cometary samples. High-speed capture left some components in excellent condition, whereas others were severely altered. In general, components larger than micron-size were often well

preserved, whereas smaller or finer-grained components were strongly modified. The most extreme modifications observed were the cases of vesicular silica in the upper regions of track walls that contain only a percentage of projectile material, usually Mg, Al, Ca, Mn, and Fe in roughly solar relative proportions, dissolved into previously molten aerogel. This glass usually contains large numbers of submicron beads of FeNi sulfide or metal, immiscible phases that could not dissolve in silica. These materials were clearly heated above the ~2000 K melting point of silica, and this is the possible fate of many of the submicron components that stopped in the upper regions of tracks.

Despite laboratory simulation studies and aerogel capture of meteoroids in space, the capture effects on bona fide comet dust at 6 km/s were unknowable before the encounter because of the unknown nature of cometary materials and the technical limitations of accelerating loosely bound aggregates like those implied by studies of interplanetary dust particles (IDPs) and meteors. Simulations at 6 km/s were done with a variety of solid particles that could be accelerated, and there was a moderate amount of experience with capture of actual meteoroids by orbiting spacecraft (5, 6). All of these projects showed that solid particles >10 μ m could be captured in reasonably good condition consistent with the Stardust mission findings. These projects showed that even temperature-sensitive materials such as hydrated silicates and materials that melt at ~600°C could be captured in good shape with only minor alteration except at particle surfaces where they were sometimes coated with a thin layer of melted aerogel. The juxtaposition of melted and unmelted material indicates extremely high temperature gradients at particle surfaces. Particles impacted Stardust at 6.1 km/s and were stopped on time scales ranging from a microsecond to less than a nanosecond depending on the particle size and the collection media. At nanosecond interaction times, the thermal wave produced by contact with molten aerogel at temperatures >2000 K does not penetrate deeply into captured particles (Fig. 3). Although the smallest components were often strongly heated, those over a micron in size appear to have been protected by their own thermal inertia.

The range of effects inside aerogel tracks can be crudely understood in terms of velocity-dependent heating. If an ideal nonfragmenting particle simply sweeps up aerogel in its path, accelerating it to the particle velocity and then releasing it, the particle's speed will decrease by 1/e every time it sweeps up its own mass of aerogel. In this simplified model, the speed (v) of a 10- μ m density 3-g/cc particle in 0.01 g/cc (ρ) aerogel decreases to 2.2 km/s after 3 mm, 0.8 km/s at 6 mm, and stops at about 1 cm when the dynamic pressure ($\sim \rho v^2$) is matched by the aerogel's compression strength. The power generated varies as v^3 , and at 3-mm and 6-mm depth it would be 5% and 0.2%, respectively, of the power generated at the point of entry. Entering projectiles generate a spray of molten aerogel that forms and lines track walls, but this process rapidly declines with depth. Aerogel along the track walls varies from molten at the entry to compressed in the mid-range and then is little affected as the track actually narrows to the projectile diameter near the track's end. Actual tracks of particles made by 10 μ m silicates are about 1 mm long, which implies somewhat faster deceleration than in this crude model. Deceleration of actual particles can be greater if the

column cross-section of aerogel that is accelerated is larger than the projectile cross-section or less if intercepted aerogel is not accelerated to the projectile velocity. Additional complications include build-up and shedding of caps (7) of compressed or melted aerogel and general fragmentation.

Context. The work on the Stardust mission samples has only recently begun, but the first laboratory studies of comet samples have already provided considerable insight into (i) the formation of comets, (ii) the origin of crystalline silicates around stars that form planets, and (iii) large-scale mixing in the solar nebula and, by inference, mixing in circumstellar accretion disks that form planets around other stars. There have been various suggestions for the origin of comets, but the most widely held view is that they are mixtures of ice and interstellar grains, specifically submicron-sized core-mantle grains (8, 9). Complicating factors to this model include infrared spectral evidence that comets, particularly long-period comets, contain crystalline silicates (10, 11), whereas silicates observed in the interstellar medium are almost entirely noncrystalline (12, 13), a state commonly attributed to radiation processes. The standard explanation for this is that crystalline silicates in comets were produced by annealing, the devitrification of glass or amorphous silicates at elevated temperature. For common silicates and appropriate time scales, this process requires temperatures of 800 K or more and is inconsistent with the environment that produced comets containing ices that condensed below 40 K. Bockelée-Morvan *et al.* (14) suggested that the annealing of amorphous silicates occurred in hot inner regions of the solar nebula and were carried outward by turbulent mixing, potentially a very effective transport process (15). Modeling suggests that turbulent mixing can cause large-scale radial mixing on 10^4 -year time scales. Although mixing is a prediction of several solar system formation models, the radial variations of the properties of minor planets as well as larger-scale variation of solar system bodies suggest that the solar nebula was not well mixed.

A major portion of the Stardust mission particles larger than a micron is composed of the silicate minerals olivine and pyroxene (Figs. 2 to 4). The presence of these two phases has also been indicated by infrared data from other comets, in particular in Hale-Bopp (11) and Tempel 1, the comet impacted by the Deep Impact mission (16). Like all minerals, and by definition of the word mineral, these are crystalline solids. There are also amorphous silicates in some of the samples, but it is not yet clear whether these existed before collection or were produced during the capture. Isotopic work on these samples is just beginning, but it is evident that the majority of the large crystalline silicates collected by Stardust have solar isotopic compositions and not the anomalous ones expected

and seen in interstellar grains. At this early stage, it appears that a major fraction of the micron and larger silicates in Wild 2 were produced in our solar system. It is also remarkable that so many of the impacting comet particles contained at least a few relatively large solid grains, an order of magnitude larger than the size of typical interstellar grains (17). In addition to silicates and abundant sulfides, the collected comet samples contain organic materials (18) even in the sub-micron size range (Fig. 5).

The range of compositions of olivine and pyroxene grains in the Stardust mission samples, particularly with regard to the minor elements, indicates a reasonable similarity to components found in interplanetary dust and some primitive unequilibrated meteorites (19). Extensive work has been done on these meteoritic materials, and there has been vigorous debate about which grains are primary condensates from hot regions of the solar nebula and which ones are fragments of highly processed materials such as chondrules, objects composed of crystals, and glass formed by rapid crystallization of a melt. In stark contrast to astronomical interpretations, studies of meteoritic materials have not suggested that these phases formed by annealing of presolar amorphous silicates. The detailed quantitative evaluation of a large set of silicates collected by Stardust has yet to be done, but the isotopic composition, minor element composition, and even the range of Fe/Si does not appear to be compatible with an origin by annealing of radiation-damaged interstellar silicates. Specifically, many of the olivines are nearly Fe free and yet have moderately high abundances of Al, Ca, Cr, and sometimes Mn. There is no model or set of ex-

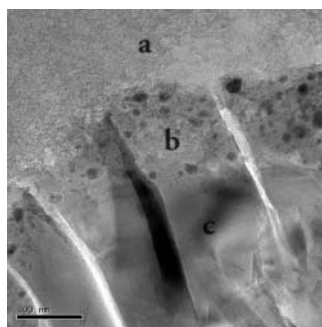


Fig. 3. Conventional brightfield transmission electron microscope image of a microtome section of an Fe99 (Mg/Mg + Fe atomic ratio = 0.99) olivine grain showing a 100-nm-thick alteration rim produced during high-speed capture. The rim (b) contains nanophase FeNi metal and sulfide grains resulting from the interaction of the grain with a thin flow of material containing Fe, Ni, and S, presumably a mix of melted silica aerogel and comet materials. Below the thin rim (c), the grain appears to be perfectly preserved; above the rim (a) is unmodified aerogel in which the particle was captured.

periments that suggest that such compositions would form from plausible amorphous interstellar materials. The composition of the grains collected by Stardust provides both a rich source of new

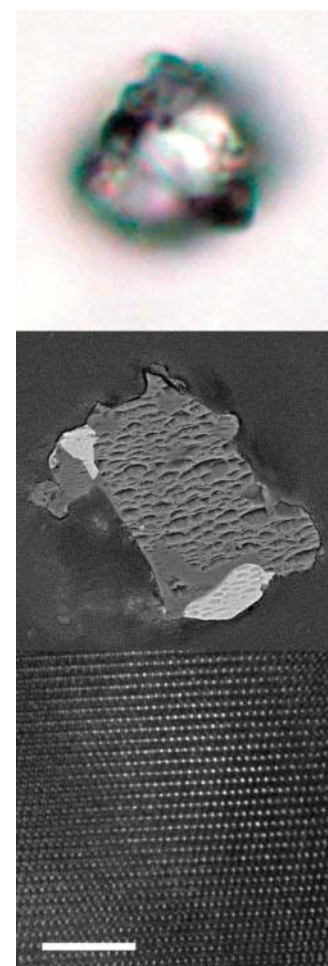


Fig. 4. Three images of the 8- μ m terminal particle at end of the >2-mm-long track 27 (Sitara), also shown in Fig. 1. The top is an optical image showing parent central grain (that is also birefringent) with two attached opaque phases. Other focus depths show additional opaques inside the grain. The middle image is an SEM backscattered electron (BSE) image of the flat surface ("potted butt") of the particle mounted in acrylic after several dozen 70-nm slices had been removed with a diamond microtome. The image brightness is proportional to mean atomic weight and this, along with x-ray spectral measurements, shows that the particle is a solid rock composed of at least four phases. The two bright regions are sulfides; one is pyrrhotite Fe_{1-x}S , and the other is pentlandite, a Ni-rich sulfide. The central gray region marked by aligned "chatter pits" from the diamond knife is enstatite. The smooth gray regions are an undetermined crystalline Mg silicate that contains Na, Al, and Ca at abundances of several percent. The bottom image shows the enstatite grain observed in a microtome section at near atomic-scale resolution. Scale bar, 5 nm).

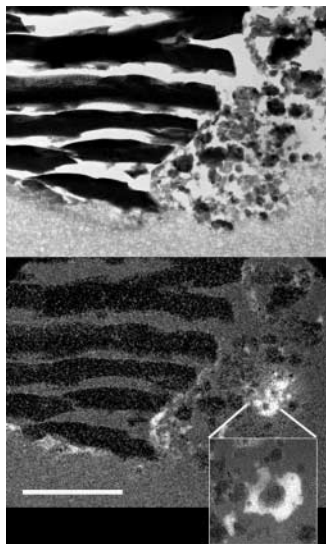


Fig. 5. Energy-filtered TEM images of the lower region of the T57 (Febo) slice shown in Fig. 2 (scale bar, 1 μm). The top image is a zero-loss image made with electrons that did not lose energy during passage through the sample, and the lower image displays the carbon distribution. The carbon image was made with the standard three-window method that combines images taken in energy passbands above and below the 285-eV carbon edge. The sulfide on the left is carbon free, but regions of carbon are seen both as submicron components in the fine-grained chondritic component on the right and as partial rims on the sulfide grain. Isotopic measurements made at Johnson Space Center have shown considerable ^{15}N enrichment in the carbon-rich region shown in the expanded window.

information for determining the origin of silicates in comets formed at the edge of the solar nebula and a superb means of assimilating and fostering new understanding of the sometimes incompatible inferences from the extraterrestrial sample and astronomical communities.

Radial mixing in the solar nebula. Perhaps the most straightforward result of the Stardust analysis program is information for large-scale mixing in the solar nebula. The comet samples collected by Stardust do contain presolar materials, the initial building materials of the solar system, but they clearly are not just a collection of submicron interstellar grains. The collection contains abundant high-temperature minerals such as forsterite (Mg_2SiO_4) and enstatite (MgSiO_3). It also contains at least one particle that is mineralogically and isotopically linked to meteoritic calcium- and aluminum-rich inclusions (CAIs). CAIs are the oldest samples of the solar system, they are systematically enriched in ^{16}O , and they contain abundant minerals that condense at temperatures higher than the 1400 K condensation temperature of forsterite. Meteoritic CAIs are thought to have formed in the hottest portion of the solar nebula. A popular model for the ^{16}O enrichment involves

photochemical self-shielding processes that may have occurred mainly in the innermost regions of the solar nebula, well inside the orbit of Mercury (20). These apparent inner solar system materials in the comet must have been transported beyond the orbit of Neptune by a process that was capable of moving particles at least as large as 20 μm . The existence of such a process provides a fundamental constraint on models of the solar nebula. Particles could have been transported from the center to the outer edge of the nebula in two different ways: (i) ballistic transport above the nebular midplane or (ii) turbulent transport in the midplane. Although it was widely believed that comets were isolated from inner solar system materials, there have been several suggestions that such transport was possible. Bockelée-Morvan *et al.* (14) and others predicted such transport based on turbulent mixing in the solar nebula disk, and Shu *et al.* (21) predicted that even quite large particles could be launched by an out-flow called the X-wind from a region that was very close to the young Sun and ballistically transported above the midplane of the nebular disk. Shu and colleagues specifically predicted that the X-wind model would transport CAIs from near the Sun to the edge of the solar system where Wild 2 formed.

Comparison with Deep Impact results. The Deep Impact mission also provided important information about the composition of dust from another Jupiter family comet. A portion of the Deep Impact spacecraft impacted comet 9P/Tempel 1 liberating $\sim 10^6$ kg of debris that was observed in the infrared. Many of the spectra have superb signal-to-noise ratios and show numerous features caused by emission from submicron grains. The Deep Impact data was used to estimate the mineralogical make-up of the comet by synthesizing the observed spectra as a mixture of spectra of various laboratory compounds (16). The model composition expressed as relative weighted surface area is ferrosilite (FeSiO_3) 33, forsterite (Mg_2SiO_4) 31, amorphous olivine [$(\text{Mg,Fe})_2\text{SiO}_4$] 17, niningerite [$(\text{Mg,Fe})\text{S}$] 15, smectite nontronite (a hydrated silicate) 14, diopside ($\text{CaMgSi}_2\text{O}_6$) 12, orthoenstatite (MgSiO_3) 10, fayalite (Fe_2SiO_4) 9, siderite (FeCO_3) 5, amorphous pyroxene [$(\text{Mg,Fe})\text{SiO}_3$] 4, and magnesite (MgCO_3) 3. Of these minerals, only forsterite was found in Wild 2 at abundances above a few percent. The inferred presence of MgFe sulfides, the oxymoron phases amorphous olivine and pyroxene, as well as carbonates and hydrated silicates are clearly at odds with the sample return data. To date, no compelling evidence has been seen in the samples for either the presence of these phases or their thermal decomposition products. For example Mg-, Ca-, or Fe-bearing carbonates, even if they decomposed during capture, would be converted to oxides by strong heating and would be readily observed if they had existed in Stardust samples. Iron sulfides are abundant components in Wild 2, but FeMg sulfides have not been seen, they are not present in IDPs, and they are exceedingly rare in primitive

meteorites. The Deep Impact modeling included components of amorphous olivine and pyroxene, yet noncrystalline silicates with these stoichiometric compositions are not seen except perhaps as trace occurrences in Wild 2, IDPs, or meteorites. The most notable difference between the results of the two missions is the presence of carbonates and hydrated silicates, phases whose existence in meteorites is usually attributed to formation by hydrothermal alteration inside a wet parent body. Extraterrestrial hydrated silicates have been collected in meteoroids impacting aerogel on Earth-orbiting spacecraft and in laboratory simulation experiments (22, 23), but they have not been seen in Stardust samples. If abundant hydrated silicates >200 nm existed in Wild 2, there should be clear evidence of them in the analyzed samples.

There are several possible explanations for the differences between the conclusions of the two missions. The comets may be different, the sampling regions are different, the size-range sampled is somewhat different, the laboratory materials that were chosen to match the observations may not be appropriate analogs for submicron cometary materials that are both ancient and complex, and numerous factors may complicate the combination of more than a dozen different components to accurately infer the mineralogical composition of a complex natural material. Comets are collections of materials that accreted to form them. It is possible that some comets contain hydrated silicates from the nebula or from the break-up of larger (>100 km) bodies that experienced internal heating, melting of ice, and aqueous alteration of silicates. The Tempel 1 sampling site was near two large features that look like impact craters, and it is conceivable that hydrated silicates could have formed inside Tempel 1 by hydrothermal processes caused by these events. Unlike Tempel 1, Wild 2 does not show clear evidence for classic impact craters, implying that its ancient cratered surface, and possible impact-modified material, has been lost due to cometary activity. As previously mentioned, Stardust is believed to have sampled particles ejected from dozens of ice-bearing subsurface regions that have never been sufficiently heated to cause the separation of the fine-grained mix of submicron dust and ice, let alone hydrothermal alteration processes that can form hydrated silicates.

Remarks. The Stardust mission has provided us large numbers of particles that were at the edge of the solar system at the time of its formation. Efforts have just begun to compare these with meteoritic samples: meteorites, ~ 0.1 -mm micrometeorites (24), and 10- μm interplanetary dust. The total mass of collected comet material is actually equivalent to several hundred thousand of the nanogram IDPs that have been intensively studied in the laboratory for the past 35 years. We anticipate that the comet samples and their comparison with meteoritic samples will provide important boundary conditions for models of the origin of the solar

system, the origin of silicate minerals around stars, and mixing in circumstellar disks. The mineral grains and components that we have seen in the comet are analogous to glacial erratics; they clearly did not form in the environment they were found in. Each particle is a treasure that provides clues on its place of origin and mode of transport. In many cases, it appears that they formed in the center of the solar nebula, and many of the larger particles are rocks composed of several minerals. Although better estimates will come from continued studies, initial investigations indicate that on the order of 10% or possibly more of the comet's mass was transported outward from the inner regions of the solar nebula as particles larger than a micron. The solar nebula may not have been well mixed, but the Stardust mission results show that there was abundant radial transport of solids on the largest spatial scales. One of the most surprising findings has been that we have seen many of these materials before. The distribution of minor element compositions of minerals, such as forsterite, indicate a link to the rare forsterite fragments found in primitive meteorites. Meteorite studies indicate that these high-temperature phases, serving as tracers, were distributed to varying degrees, sometimes as very minor components, across the inner parts of the solar nebula (25–27). From the work on Stardust samples, it now appears that components like forsterite and CAIs, formed in the hottest regions of the solar nebula, were transported over the entire solar nebula.

Comets have always been notable because of their contents of frozen volatiles but they are now additionally notable because of their content of exotic refractory minerals. The information on materials and mixing from the Stardust mission provide a new window of insight into the origin of solid grains that form disks around stars and lead to the formation of planetary bodies. This is a window that is explored with electron microscopes, mass spectrometers, synchrotrons, and a host of other modern instruments to provide information at levels of detail that were not previously imagined. The best available instruments and methods on the planet were used in this study, and it is expected that additional studies coupled with advances in analytical capabilities will continue to reveal important secrets about the origin and evolution of the solar system that are contained in these few thousand particles recovered from comet Wild 2.

References and Notes

1. D. E. Brownlee *et al.*, *Science* **304**, 1764 (2004).
2. Z. Sekanina *et al.*, *Science* **304**, 1769 (2004).
3. H. F. Levison, M. J. Duncan, *Icarus* **127**, 13 (1997).
4. D. R. Davis, P. Farinella, *Icarus* **125**, 50 (1997).
5. F. Horz *et al.*, *Science* **314**, 1716 (2006).
6. F. Horz *et al.*, *Icarus* **147**, 559 (2000).
7. G. Dominguez *et al.*, *Icarus* **172**, 613 (2004).
8. J. M. Greenberg, in *Comets*, L. L. Wilkening, Ed. (Univ. of Arizona Press, Tucson, 1982), pp. 131–163.
9. J. M. Greenberg, *Astron. Astrophys.* **330**, 375 (1998).
10. M. S. Hanner *et al.*, *Astrophys. J.* **425**, 274 (1994).
11. D. H. Wooden *et al.*, *Astrophys. J.* **517**, 1034 (1999).
12. F. Kemper, W. J. Vriend, A. G. G. M. Tielens, *Astrophys. J.* **609**, 826 (2004).
13. J. Dorschner *et al.*, *Astron. Astrophys.* **300**, 503 (1995).
14. D. Bockelée-Morvan *et al.*, *Astron. Astrophys.* **384**, 1107 (2002).
15. J. N. Cuzzi, S. S. Davis, A. R. Dobrovolskis, *Icarus* **166**, 385 (2003).
16. C. Lisse *et al.*, *Science* **313**, 635 (2006).
17. J. S. Mathis *et al.*, *Astrophys. J.* **217**, 425 (1977).
18. S. A. Sandford *et al.*, *Science* **314**, 1720 (2006).
19. Unequilibrated meteoritic materials have not experienced substantial diffusion of atoms between components, usually due to heating, that causes phases such as olivine to have the same elemental composition. The wide range of Fe/Mg ratios in Wild 2 olivine as well as the Ni content of sulfides show that the comet is at least as unequilibrated as the very rare and least equilibrated meteorites.
20. R. N. Clayton, *Nature* **415**, 860 (2002).
21. F. H. Shu *et al.*, *Astrophys. J.* **548**, 1029 (2001).
22. K. Okudaira, *36th Annual Lunar and Planetary Science Conference* **36**, 1832 (2005).
23. G. A. Graham *et al.*, *Dust in Planetary Systems*, Proceedings of the conference held 26 to 28 September 2005 in Kaua'i, Hawaii. LPI Contribution No. **1280**, 56 (2005).
24. C. Engrand *et al.*, *Meteoritics Planet. Sci.* **41**, 5237 (2006).
25. E. R. D. Scott, A. N. Krot, *Astron. Soc. Pacific Conf. Ser.* **341**, 15 (2005).
26. A. Pack, H. Palme, J. M. G. Shelley, *Geochim. Cosmochim. Acta* **69**, 3159 (2005).
27. S. Simon, L. Grossman, *Meteoritics Planet. Sci.* **38**, 813 (2003).
28. The Stardust sample analysis team is grateful to NASA for funding and supporting the mission and to the hundreds of other team members that were involved in design, construction, flying, and recovery of the mission. The team, from 100 organizations, gratefully acknowledges their supporting institutions.

3 October 2006; accepted 17 November 2006
10.1126/science.1135840

REPORT

Impact Features on Stardust: Implications for Comet 81P/Wild 2 Dust

Friedrich Hörz,^{1*} Ron Bastien,² Janet Borg,³ John P. Bradley,⁴ John C. Bridges,⁵ Donald E. Brownlee,⁶ Mark J. Burchell,⁷ Miaofang Chi,⁴ Mark J. Cintala,¹ Zu Rong Dai,⁴ Zahia Djouadi,³ Gerardo Dominguez,⁸ Thanasis E. Economou,⁹ Sam A. J. Fairey,⁷ Christine Floss,¹⁰ Ian A. Franchi,⁵ Giles A. Graham,⁴ Simon F. Green,⁵ Philipp Heck,¹¹ Peter Hoppe,¹¹ Joachim Huth,¹¹ Hope Ishii,⁴ Anton T. Kearsley,¹² Jochen Kissel,¹³ Jan Leitner,¹⁴ Hugues Leroux,¹⁵ Kuljeet Marhas,¹⁰ Keiko Messenger,² Craig S. Schwandt,² Thomas H. See,² Christopher Snead,¹⁶ Frank J. Stadermann I,¹⁰ Thomas Stephan,¹⁴ Rhonda Stroud,¹⁷ Nick Teslich,⁴ Josep M. Trigo-Rodríguez,^{18,19} A. J. Tuzzolino,⁹ David Troadec,²⁰ Peter Tsou,²¹ Jack Warren,² Andrew Westphal,¹⁶ Penelope Wozniakiewicz,¹² Ian Wright,⁵ Ernst Zinner¹⁰

Particles emanating from comet 81P/Wild 2 collided with the Stardust spacecraft at 6.1 kilometers per second, producing hypervelocity impact features on the collector surfaces that were returned to Earth. The morphologies of these surprisingly diverse features were created by particles varying from dense mineral grains to loosely bound, polymineralic aggregates ranging from tens of nanometers to hundreds of micrometers in size. The cumulative size distribution of Wild 2 dust is shallower than that of comet Halley, yet steeper than that of comet Grigg-Skjellerup.

Stardust's sample collector exposed SiO₂-based aerogel and aluminum foil to the flux of particles emanating from comet Wild 2 as the spacecraft's trajectory took it to within 234 km of the comet's surface (1).

The cometary dust grains collided with these surfaces at 6.1 km s⁻¹, producing hypervelocity craters in the aluminum and deep penetration tracks in the highly porous, low-density aerogel (2) (fig. S1). Even the most cursory inspection

of these surfaces reveals an unexpected diversity in the morphologies and sizes of both craters and tracks.

Detailed morphologic analysis of these impact features and comparison with experimental impacts produced by a suite of well-characterized projectiles was undertaken during the preliminary examination of Stardust to evaluate the common view that cometary solids are fluffy, highly porous objects (3). Also, the size distribution of Wild 2 dust can be deduced from the size distribution of the impact features and compared with those for other comets, such as Halley (4). In addition, attempts were made to analyze the compositions of molten projectile residues inside craters, as detailed by Zolensky *et al.* and Flynn *et al.* (5, 6).

Stardust's fixed encounter speed of 6.1 km s⁻¹ is well within the performance limits (~7 km s⁻¹) of small-caliber, light-gas guns, allowing direct laboratory simulation of Stardust's impact features (7–9). This is in stark contrast to earlier dust-collection experiments in low Earth orbit, which included aluminum (10) and SiO₂-based aerogel (11, 12). Figure 1 compares experimental craters into Al₁₀₀₀ targets with those observed on Stardust foils and shows that detailed crater morphology reflects the physical properties of the impactor(s). It also illustrates